17th World Conference on Earthquake Engineering, 17WCEE
Sendai, Japan - September 13th to 18th 2020

Structural Performance of RC Beams with Induced Corrosion Cracks by Aluminum Pipe Filled with an Expansion Agent

T. Aburano[1], A. S. Syll[2], T. Kanakubo[3]

[1] *Graduate Student, Graduate School of Systems and Information Engineering, University of Tsukuba, s1920881@s.tsukuba.ac.jp*
[2] *Graduate Student, Graduate School of Systems and Information Engineering, University of Tsukuba, s1820961@s.tsukuba.ac.jp*
[3] *Professor, Department of Engineering Mechanics and Energy, University of Tsukuba, Dr. E, kanakubo@kz.tsukuba.ac.jp*

Abstract

In Japan, many reinforced concrete (RC) structures built in 1960-70's. Some of them are facing damages due to bar corrosion. Corrosion causes the reduction of the cross section of reinforcing bar and also concrete cracks. Many researchers focused on the influence of cracks in concrete due to bar corrosion. The electrolytic corrosion or slits insertion methods have been used to simulate the cracking of concrete in many previous studies. Authors have proposed a new crack simulation method by using an expansion agent filled pipes (EAFP). When the expansion agent is mixed with water and filled inside a pipe, expansion pressure can cause the cracking of concrete. Cracking mechanism is very close to one due to internal pressure by corrosion products. The purpose of this study is to evaluate the influence of cover concrete cracks due to bar corrosion on bond behavior between bar and concrete.

First, the possibility to simulate cracks by EAFP is investigated. A specimen with the same cross section than one designed for the anti-symmetrical bending moment test is adopted. According to the results of the cracks simulation test, cracks were observed along the main bars by EAFP. To better examine the internal cracks, a transversal cut of the specimen was performed. Side split type cracks and corner split type cracks were observed.

Finally, the anti-symmetrical bending moment loading test using specimens with induced cracks by EAFP is carried out. According to the results, the difference of crack width induced by EAFP before loading did not significantly affect the maximum capacity. However, translational angle at the maximum load tends to increase as the crack width before loading increased. Comparing shear force – translational angle curves up to 1/100 rad, the decrement of stiffness of the specimen with large level of cracks is remarkably greater than those of specimen with small level of cracks. In the curves after 1/50 rad, there are no clear relations between the reduction of shear force and induced crack width before loading. Stiffness reduction greatly affects the reduction of accumulated energy absorption due to bond deterioration of main bars in specimen with induced crack width of about 1.5mm.

Keywords: bar corrosion; bond behavior; expansion agent; anti-symmetrical bending moment loading

1. Introduction

A lot of reinforced concrete (RC) structures were built in the 1960s in Japan, and it is feared that these structures are damaged by bar corrosion. Bar corrosion causes a reduction of cross section of bar and cracks in concrete. Recently, many studies have researched on the relationship between bar corrosion and the structural performance of RC members. The previous study [1] carried out anti-symmetrical bending moment loading by using the exposed column specimens. It has been suggested that the maximum load and energy absorption capacity of the exposed specimens decreases due to a reduction of cross section of bar. However, comparing the crack situation of specimens before and after loading, the localized damage is observed at the cracked area before loading. It is considered that cracks in concrete due to bar corrosion also affect the structural performance of specimens.

In the previous research, exposure tests and electrolytic corrosion tests have been generally conducted to simulate corrosion cracks. However, these methods have disadvantages such as needs of long duration for test or difficulty of controlling cracks. The authors have proposed the simulation method to cause same crack as bar corrosion using an expansion agent filled pipe (EAFP) [2]. Cracks can be obtained by this method in short duration comparing to electrolytic corrosion test, and a target of crack width can be controlled by the elapsed time from filling expansion agent. It has been reported that the average crack width of RC beams using EAFP instead of compression bar was 0.5~1mm after 300 hours from filling agent [3]. This study has suggested that corrosion cracks does not significantly affect pure bending behavior by the monotonous bending loading of the specimens with cracks on the compression side.

The purpose of this study is to evaluate the influence of cover concrete cracks due to bar corrosion on the bond behavior between bar and concrete. At first, the simulation test to observe the cracks by EAFP is conducted by using the specimens which have same cross section as specimens of the anti-symmetrical bending moment loading test. Next, the anti-symmetrical bending moment loading test using specimens with induced cracks by EAFP is performed and the effects of corrosion cracks on the bond behavior and energy absorption capacity are discussed.

2. Cracks simulation test using EAFP

2.1 Specimens

Table 1 shows the list of specimens, and Fig.1 shows arrangement of bars. Four specimens were tested. Cross section is set as 220mm x 420mm which is same as that of specimens for the anti-symmetrical bending moment loading test. An aluminum pipe with an outer diameter of 22mm and thickness of 1mm was placed at the four corners of the specimens, and two deformed reinforcing bars were placed at the top and bottom of the cross section. An expansion agent is filled into pipes after 4 weeks later from concrete casting. Both ends of the specimen is reinforced by stirrups (D6@30). The specimen lengths are 840mm and 1260mm, where 1260mm is the same as the clear span of the specimens for the anti-symmetrical bending moment loading test. Cracks in specimens S-84 and S-126 were observed visually and measured by a crack scale, and the crack width was measured by π-type LVDTs located at cracks in specimens P-84 and P-126.

Normal concrete with 20mm maximum size aggregate was used. The compressive strength of the concrete was 24.5MPa and elastic modulus was 19.8GPa when an expansion agent was filled. An aluminum pipe with outer diameter of 22mm and thickness of 1mm was used as EAFP.

Table 1 – List of specimens

No.	Specimen ID	Crack measuring method	Specimen lengths (mm)
1	S-84	Visual and a clack scale	840
2	S-126		1260
3	P-84	π-type LVDTs	840
4	P-126		1260

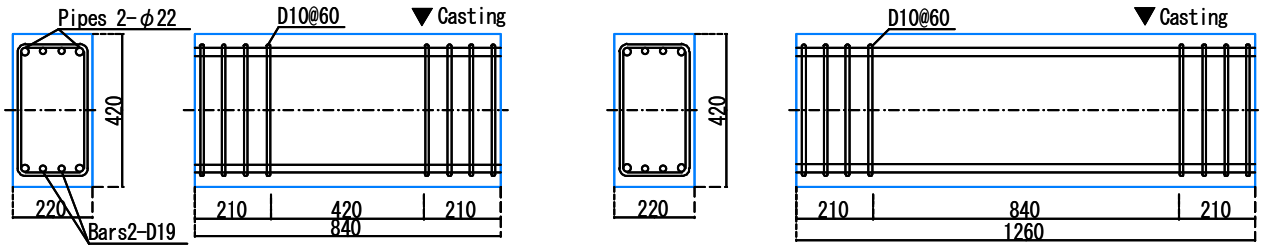

Fig.1 – Arrangement of bar

2.2 Results of cracks simulation test

Fig.2 shows specimens S-84 and S-126 at 300 hours after filling with an expansion agent. The crack width was measured using a crack scale along the aluminum pipe in three sections in no-stirrup region. The values in the figures show the maximum crack width measured in each section. Cracks were induced along the pipes by an expansion agent in all specimens. In the long specimen, there was almost no difference in the crack width between the upper and lower bars. In the short specimen, crack width was larger in the upper bars than that in the lower. It is considered that there was the effect of the crack due to concrete settling at the upper bars.

After measuring the cracks in specimens S-84 and S-126, these specimens were cut at the center, and the cross section was observed. Fig.3 shows the cut surface of each specimen. It was found that cracks were also generated inside the specimens by EAFP. In specimen S-84, there were side split type cracks around the upper and lower bars. In specimen S-126, there was side split type crack around the upper bars and corner split type cracks around the lower bars.

Fig.4 shows the results of measuring the crack width from the filling of an expansion agent to 300 hours after by using π-type LVDTs in specimens P-84 and P-126. π-type LVDTs were installed at two symmetrical positions for one crack. Total of eight π-type LVDTs were installed for the upper and lower bars on the front and back side of the specimen. The average of two data measured at the same bar is plotted in the graph. The temperatures every 10 hours by Japan Meteorological Agency at Tsukuba station are also plotted. Because of concrete settling cracks at upper bar position, the measurement was started after measuring those crack width by a crack scale when an expansion agent was filled. At about 50 hours after filling with an expansion agent, the crack width tends to increase sharply. In particular, the tendency is remarkable at lower bar position. It is considered that concrete is more densely compacted at lower bar position rather than at upper bar position where the settling crack is occurred. The effect of temperature is not clear and the difference by test length is also not significant.

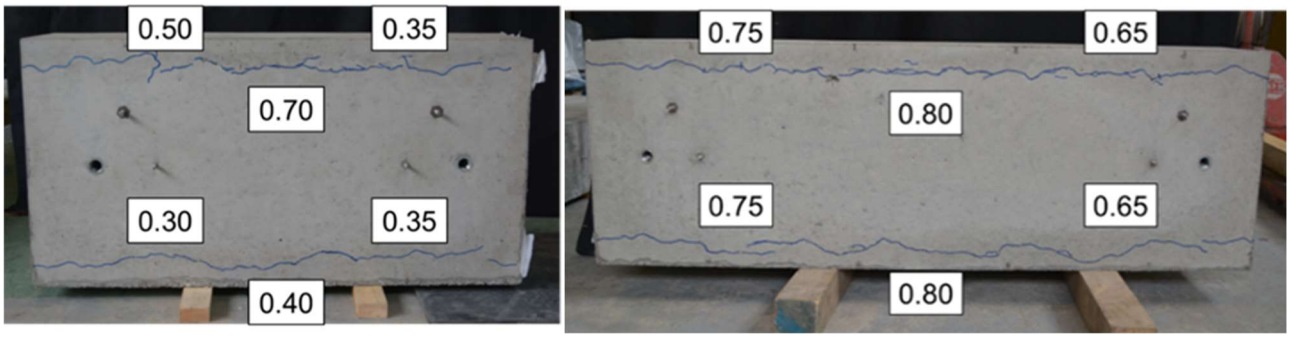

S-84 (Unit: mm) S-126 (Unit: mm)

Fig.2 – Cracks induced by EAFP

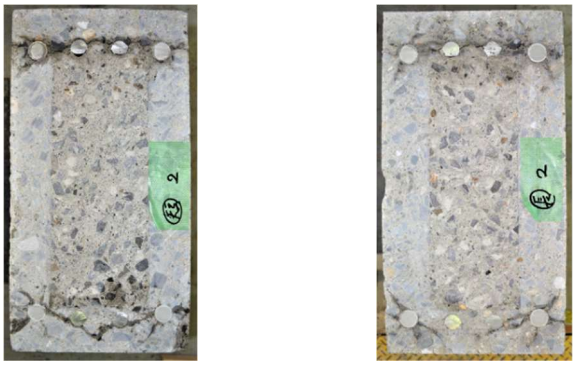

S-84 S-126

Fig.3 – Cross section of specimen

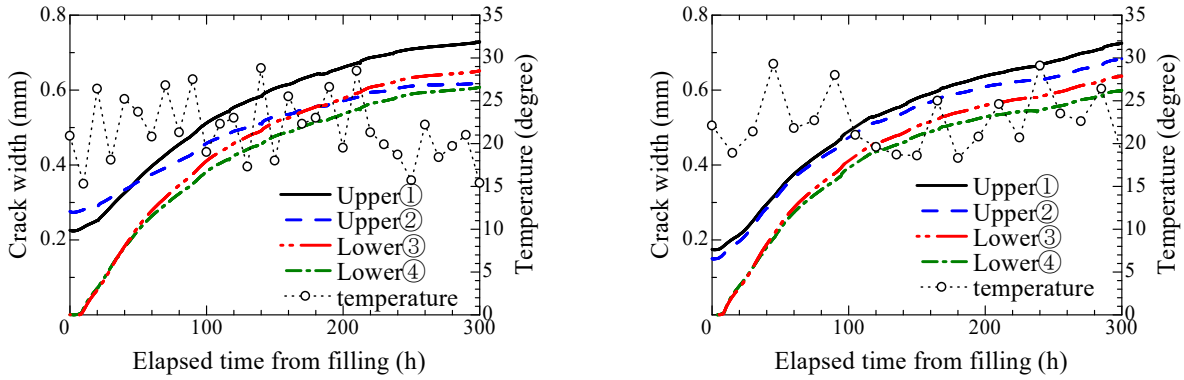

P-84 P-126

Fig.4 – Transition of crack width

3. Anti-symmetrical bending moment loading test

3.1 Specimens

Table 2 shows the list of specimens, and Fig.5 shows arrangement of bars. Three specimens were tested. Cross section is set as 220mm x 420mm which is same as specimens for the crack simulation test. The main bars are 2-D19, and the stirrups are D10@200. The test region is the central section of 1260mm, and both ends are reinforced with stirrups (D10@100). The target strength of concrete is 18 MPa. The variable factor is the target maximum crack width induced by EAFP as shown in Table 2.

Table 3 shows the calculation results of strength capacities of the specimens without considering the induced cracks. In order to confirm the bond behavior of the specimens, it was designed so that the bond failure occurs after flexural yielding. The bending strength, shear strength, and bond strength of the specimen is calculated by formulas for conventional RC members by Architectural Institute of Japan [4],[5],[6]. The effect of strength of EAFP itself was ignored. When determining the splitting line length in calculating the bond strength, aluminum pipes with outer diameter of 22mm is considered.

Table 2 – List of specimens

Specimen ID	Commons	Target maximum crack width
Level.1	Clear span: 1260mm Shear span ratio: 1.5 Stirrup ratio: 0.32%	$\omega_{cr} < 0.3$mm
Level.2		$0.3 \leqq \omega_{cr} < 0.5$mm
Level.3		$0.5\text{mm} \leqq \omega_{cr}$

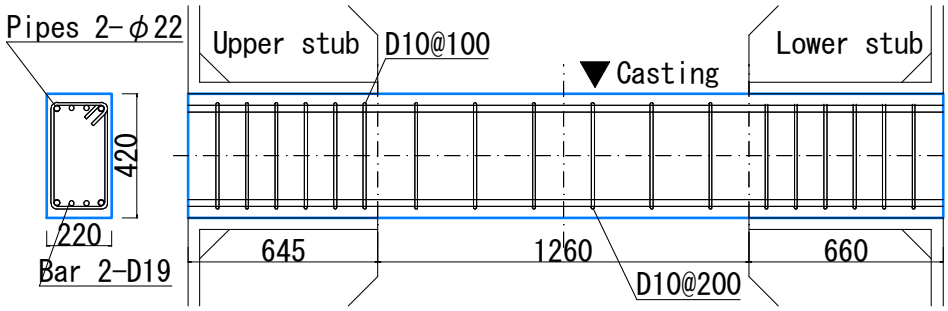

Fig.5 – Arrangement of bar

Table 3 – Calculation of capacities

Bending strength Q_{Mu} (kN)	Shear strength V_u (kN)	Bond strength V_{bu} (kN)	Shear margin index V_u / Q_{Mu}	Bond margin index V_{bu} / Q_{Mu}
111	220	179	1.99	1.62

3.2 Material test result

Normal concrete with 20mm maximum size aggregate was used. The target strength was 18MPa. Concrete was cast from the upper side of the specimen. Compression and splitting test results of concrete are listed in Table 4. The main bar is D19 and stirrup is D10. SD345 was used for D19, and SD295 was used for D10. Tensile test results of reinforcing bars are listed in Table 5. An aluminum pipe with outer diameter of 22mm and thickness of 1mm was used as EAFP. Tensile test results of the aluminum pipe are listed in Table 6.

Table 4 – Mechanical property of concrete

Target strength	Compressive strength (MPa)	Elastic modulus (GPa)	Splitting strength (MPa)
18 MPa	23.8	17.6	2.28

Table 5– Mechanical property of reinforcing bar

Type	Yield strength (MPa)	Tensile strength (MPa)	Elastic modulus (GPa)	Elongation at break (%)
D10	349	525	190	25.2
D19	366	535	193	25.4

Table 6 – Mechanical property of aluminum pipe

Yield strength (MPa)	Tensile strength (MPa)	Elastic modulus (GPa)	Poisson's ratio
176	199	61.7	0.341

3.3 Loading and measurement method

Fig.6 shows loading system. Loading method is the anti-symmetrical bending moment loading. The specimens were raised vertically, and the specimen ends were fixed with steel angles in the loading system. Axial force was controlled to 0kN and shear force was applied by100ton actuator keeping both stubs in parallel. Fig.7 shows loading history. The loading was carried out in cyclic manner by controlling translational angle. Shear force, relative displacement between stubs, axial displacement between stubs, strain of main bars, stirrups and aluminum pipes were measured. The translational angle is obtained from relative displacement between stubs divided by clear span length.

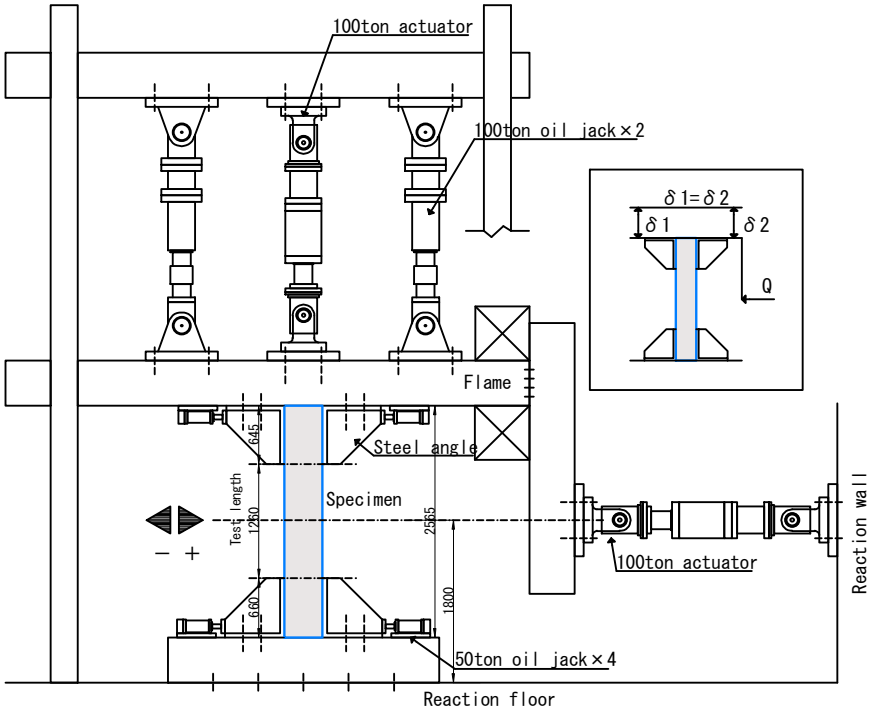

Fig.6 – Loading system

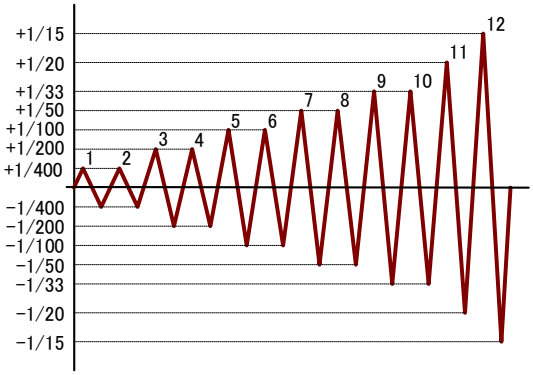

Fig.7 – Loading history

4. Results of anti-symmetrical loading test

4.1 Failure progress

Fig.8 shows crack patterns of specimens before loading and at 1/50 rad translational angle. The failure progress is described as follow:

Specimen Level.1: The cracks with a maximum width of 0.05mm were induced by EAFP. During the loading cycle of 1/400 rad, bending cracks and bending shear cracks occurred. During the loading cycle of 1/100 rad, bond splitting cracks occurred at upper bar position. The bending shear cracks and bond splitting cracks spread and finally failed by bond splitting.

Specimen Level.2: The cracks with a maximum width of 0.4mm were induced by EAFP. During the loading cycle of 1/400 rad, bending cracks and bending shear cracks occurred. During the loading cycle of 1/200 rad, bond splitting cracks occurred at upper bar position. During the loading cycle of 1/100 rad, bending shear cracks and bond splitting cracks occurred at lower bar position. The bending shear cracks and bond splitting cracks spread and failed by bond splitting similarly as specimen Level.1.

Specimen Level.3: The cracks with a maximum width of 1.6mm were induced by EAFP. During the loading cycle of 1/400 rad, bending cracks occurred. During the loading cycle of 1/200 rad, bond splitting cracks occurred at upper bar position. No new bond splitting crack observed around the induced cracks of 0.8mm width or more, only the induced cracks widened.

(a) Cracks before loading (b) Cracks at 1/50 rad

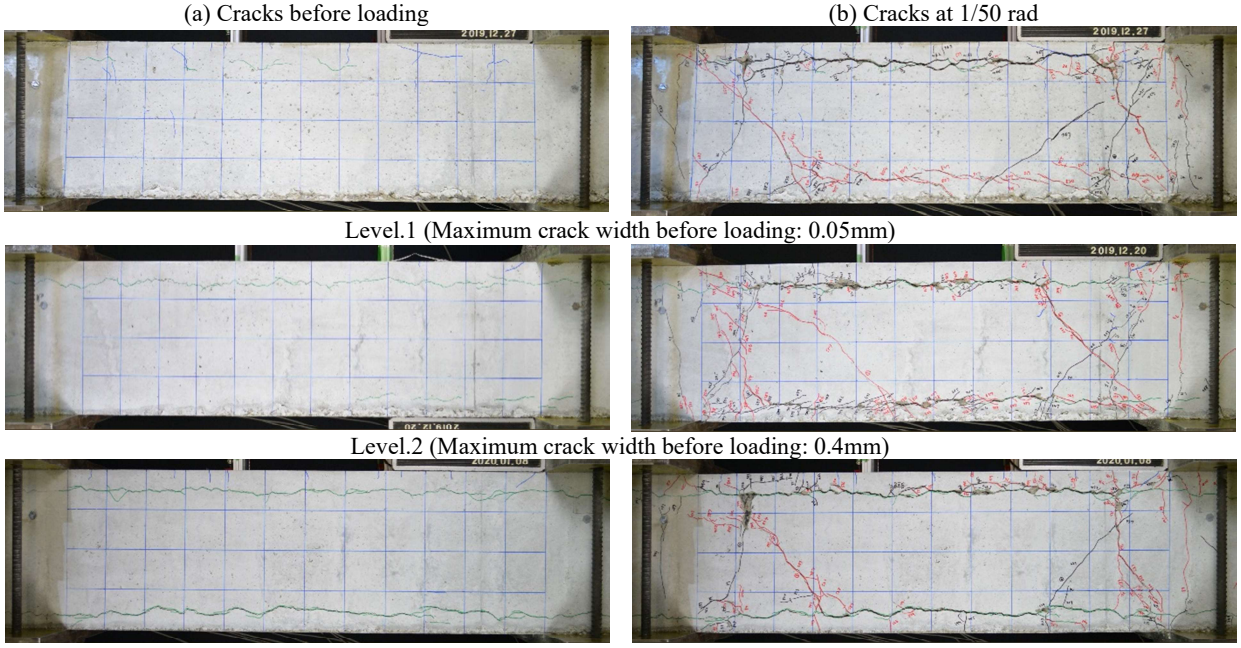

Level.1 (Maximum crack width before loading: 0.05mm)

Level.2 (Maximum crack width before loading: 0.4mm)

Level.3 (Maximum crack width before loading: 1.6mm)

Fig.8 – Crack patterns

4.2 Shear force - translational angle curve

Fig.9 shows the shear force - translational curves. Straight line shows the calculated bending strength.

Specimen Level.1: During the loading cycle of 1/100 rad, maximum shear force reached 139kN. Since there was no remarkable decrease of shear force up to 1/50 rad, it is considered that flexural yielding took the lead. After that, shear force gradually decreased due to bond splitting failure. After 1/50 rad, the hysteresis loops showed like inverted S-shape due to the slip of main bars remarkably.

Specimen Level.2: During the loading cycle of 1/100 rad, maximum shear force reached 141kN. It is considered that bond splitting failure occurred after flexural yielding similar as the case of specimen Level.1. The hysteresis loops also showed like inverted S-shape.

Specimen Level.3: During the loading cycle of 1/50 rad, maximum shear force reached 132kN. After showing maximum, shear force immediately dropped. Since there is no large difference in maximum shear force among three specimens, it is considered that bond splitting failure occurred immediately after flexural yielding. The hysteresis loops were similar with those of other specimens.

Table 7 shows the maximum capacity of shear force of each specimen, the translational angle at the maximum and these averages of the positive and negative loading directions. The difference of crack width induced by EAFP before loading does not significantly affect the maximum capacity. Since each specimen reached the maximum capacity by flexural yielding, it is considered that the induced cracks have no influence on the maximum capacity. It is observed that the translational angle at maximum tends to increase as the crack width before loading increased. It is due to the bond deterioration of main bars that causes the large opening of the bending crack and increasing of the elongation of main bars through all clear span region.

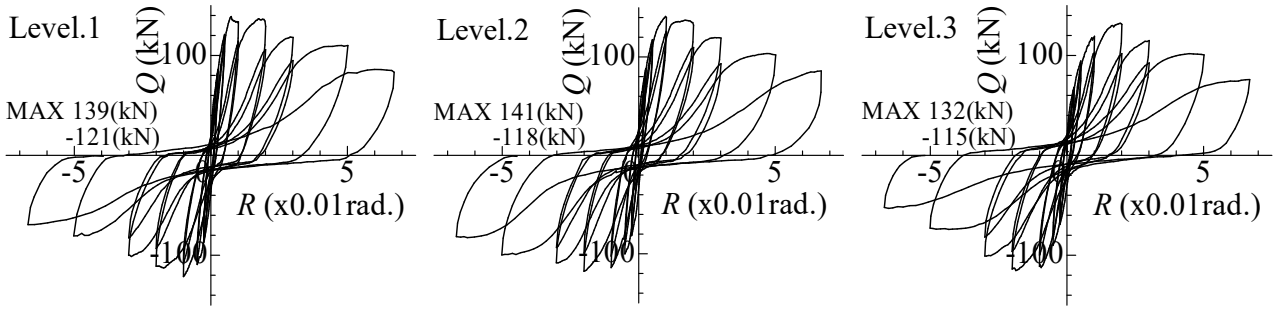

Fig.9 – Shear force - translational angle curve

Table 7 – Test results

Specimen ID	Max. capacity (+) (kN)	Translational angle (+) (x0.01rad)	Max. capacity (-) (kN)	Translational angle (-) (x0.01rad)	Ave. capacity (kN)	Ave. angle (x0.01rad)
Level.1	139	0.75	121	0.98	130	0.87
Level.2	141	0.98	118	2.01	130	1.50
Level.3	132	1.95	115	1.91	124	1.93

4.3 Comparison of skeleton curve

Fig.10 shows skeleton curves of three specimens. Comparing the curves up to 1/100 rad, it can be seen that the decrement of stiffness of specimen Level.3 is remarkably greater than that of specimens Level.1 and Level.2. This is due to the bond deterioration of main bars. In the region from 1/100 rad to 1/33 rad, the decrease in shear force of specimen Level.2 tends to decrease rather than other specimens. According to the previous research [7], up to about 3% of corrosion weight loss in electrolytic corrosion bar, the bond strength is generally increased comparing to that of non-corroded bar. This is assumed to be affected by the interlocking effect of the corrosion products. Also in this research, cracks induced in specimen Level.2 have a possibility to increase the strength.

In the curves after 1/50 rad, the differences are seen between the positive and negative loadings. At the positive loadings, the shear force decreases with the increase of translational angle. And also, the shear force largely decreases with a larger induced crack width before loading. At the negative loadings, while the shear force decreases with the increase of translational angle, there are no clear relations between the reduction of shear force and induced crack width before loading. It is considered that the effect of cracks taking place in the loading is larger than that of induced crack before loading.

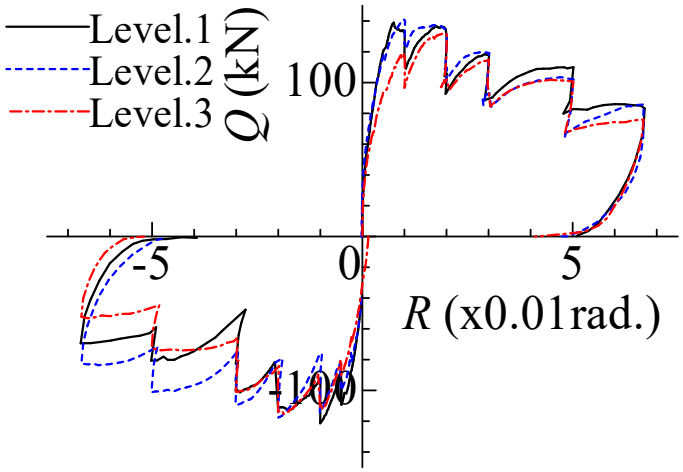

Fig.10 – Skeleton curve

4.4 Energy absorption capacity

Fig.11 shows the cumulative energy absorption ratio of each specimen based on specimen Level.1. Focusing on specimen Level.2, up to 1/400 rad, the accumulated energy absorption is larger than that of specimen Level.1. After 1/200 rad, there is no significant difference in the accumulated energy absorption between specimens Level.1 and Level.2.

Focusing on specimen Level.3, accumulated energy absorption tends to decrease greatly up to 1/100 rad. It is considered that stiffness reduction greatly affects energy absorption performance due to bond deterioration of main bars in specimen with induced crack width of about 1.5mm. After 1/33 rad, all specimens have similar energy absorption performance. It is considered that the difference of induced crack condition of each specimen disappears with failure progressing by the loading.

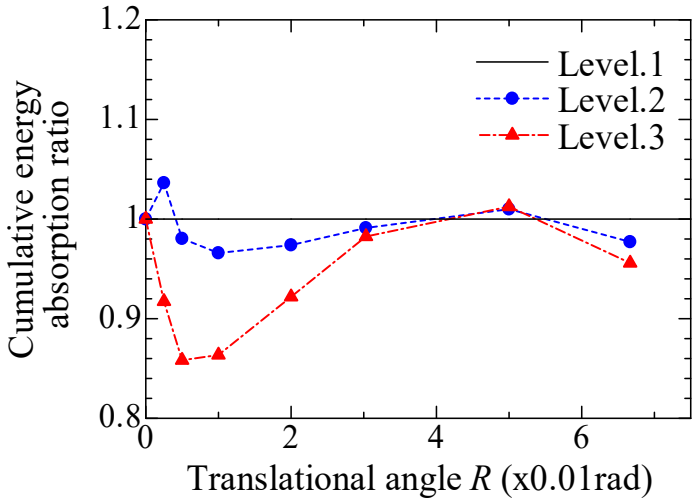

Fig.11 – Cumulative energy absorption ratio

5. Conclusions

In this study, the crack simulation test was conducted using RC members with induced corrosion cracks by EAFP. The anti-symmetrical bending moment loading test using specimens with induced cracks by EAFP was performed and the effects of corrosion cracks on the bond behavior and energy absorption capacity are discussed. The larger elapsed time after filling the expansion agent tends to increase the crack length and crack width. By using EAFP, cracks were also generated inside the specimens such as side split type crack and corner split type crack. The cracks before loading had no significant effect on the maximum capacity. However, the cracks had effect on the stiffness up to 1/100 rad and translational angle at the maximum load. In the region from 1/100 rad to 1/33 rad, the decrease in shear force of specimen with crack width of about 0.5mm tends to decrease. Stiffness reduction greatly affects the reduction of accumulated energy absorption due to bond deterioration of main bars in specimen with induced crack width of about 1.5mm.

6. Acknowledgement

This study was supported by the JSPS KAKENHI Grant Number 17K18917.

7. References

[1] Funaki, H., Yamakawa, T., Nakada, K. (2011): Experimental Studies on Durability and Seismic Performance of Real-Scaled RC Columns Exposed at A Coastal Area in Okinawa. *Journal of Structural and Construction Engineering*, Architectural Institute of Japan, Vol.76, No.666, 1479-1488.

[2] Syll, A.S., Kawamura, Y., Kanakubo, T. (2018): Simulation of Concrete Cracks due to Bar Corrosion by Aluminum Pipe Filled with An Expansion Agent, *Summaries of Technical Papers of Annual Meeting*, Architectural Institute of Japan, Structure IV, 55-56.
[3] Kawamura, Y., Kanakubo, T. (2018): Flexural Performance of RC Beams with Simulated Cracks due to Bar Corrosion by Aluminum Pipe Filled with An Expansion Agent, *Conference of Kanto Branch of JSCE* , Japan Society of Civil Engineers, V-22.
[4] Architectural Institute of Japan (2010): AIJ Standard for Structural Calculation of Reinforced Concrete Structures -Based on Allowable Stress Concept-, 611-612.
[5] Architectural Institute of Japan (1990): Design Guidelines for Earthquake Resistant Reinforced Concrete Buildings Based on Ultimate Strength Concept, 114-127.
[6] Architectural Institute of Japan (1997): Design Guidelines for Earthquake Resistant Reinforced Concrete Buildings Based on Inelastic Displacement Concept, 175-192.
[7] Japan Concrete Institute (1998): Report of Technical Committee for Rehabilitation of Concrete Structures, 47-49.

